# Spin splitting in the electron subband of asymmetric GaAs/$Al_xGa_{1-x}As$ quantum wells: The multiband envelope function approach

L. Wissinger and U. Rössler
*Institut für Theoretische Physik, Universität Regensburg, D-93040 Regensburg, Germany*

R. Winkler
*Institut für Theoretische Physik, Universität Regensburg, D-93040 Regensburg, Germany*
*and Institut für Technische Physik, Universität Erlangen-Nürnberg, Staudtstrasse 7, D-91058 Erlangen, Germany*

B. Jusserand
*France Télécom, CNET/PAB, Laboratoire de Bagneux, 196 Avenue Henri Ravera, F-92220 Bagneux, France*

D. Richards
*Cavendish Laboratory, Madingley Road, Cambridge CB3 OHE, United Kingdom*
(Received 13 July 1998)

The dependence on carrier concentration of the anisotropic spin splitting of the lowest electron subband in asymmetrically doped GaAs/$Al_xGa_{1-x}As$ quantum wells is determined. We employ the multiband envelope function approach based on $8\times8$ and $14\times14$ $\mathbf{k}\cdot\mathbf{p}$ Hamiltonians. Our self-consistent calculations yield results in quantitative agreement with experimental data obtained from inelastic light scattering.
[S0163-1829(98)04448-8]

Spin degeneracy in the single-electron energy spectra of solids is the combined effect of inversion symmetry in space and time.[1] Both symmetry operations convert the particle wave vector $\mathbf{k}$ into $-\mathbf{k}$, but time inversion flips in addition the electron spin. The lack of either spatial inversion symmetry (or likewise of a symmetry that changes $\mathbf{k}$ into $-\mathbf{k}$) or of time inversion symmetry removes the spin degeneracy. Spin splitting due to lack of inversion symmetry is well-known from early theoretical studies for bulk semiconductors with zinc-blende structure[2–4] and has been demonstrated by detecting the precession of the spin polarization of electrons photoexcited from a GaAs (110) surface.[5] In addition to this bulk inversion asymmetry (BIA) spin splitting in semiconductor quantum wells can be caused also by the asymmetry of the confining potential. It is referred to as surface inversion asymmetry (SIA), and has the meaning of spin-orbit interaction of the electron (or hole) moving in the quantum well potential.[6–9] More recently this spin-orbit or Rashba term has been proposed as possible gate control for a future spin transistor in heterojunctions based on narrow gap InAs.[10] A more direct evidence of spin splitting of the electronic subbands in quantum well structures comes from the detection of single-particle spin-flip transitions at the Fermi energy, which can be probed in inelastic light-scattering experiments with crossed polarizations of incident and scattered light. These experiments[11,12] have been performed on asymmetrically *n*-doped GaAs/$Al_xGa_{1-x}As$ quantum wells. They provide clear information on the spin splitting of the electron subband at the Fermi energy in dependence of the carrier density and on its anisotropy in $\mathbf{k}_\parallel$ space. In the present paper, we compare these experimental data with calculated spin splittings. We apply the multiband envelope function approach[13] based on $8\times8$ and $14\times14$ $\mathbf{k}\cdot\mathbf{p}$ Hamiltonians and find good quantitative agreement with the Raman data. Our results will be discussed in comparison with those recently published by Pfeffer,[8] who simulates the asymmetric quantum well by a single heterojunction. He misinterpreted the experimental data by a factor of 2 by taking the Raman spin splitting in Fig. 2 in Ref. 12 as the subband spin splitting.

A quantitative calculation of the subband dispersion in quantum wells has to take into account properly the bulk band structure of the involved semiconductors and the geometry of the quantum structure including the doping profile. The bulk band structure of GaAs belongs to the best-known single-particle spectra in solid state physics. The near band-edge states are well described by a $14\times14$ (or five level) $\mathbf{k}\cdot\mathbf{p}$ model,[3,14] which takes explicitly into account the $\Gamma_{8v}$ and $\Gamma_{7v}$ topmost valence-band states and the $\Gamma_{6c}$, $\Gamma_{7c}$, and $\Gamma_{8c}$ conduction-band states. Within this model, the parameters for which have been determined to high precision by experiment, the lowest conduction band is accurately described in the energy range of subband formation in quantum wells. Almost as accurate knowledge exists about the $\mathbf{k}\cdot\mathbf{p}$ parameters for the barrier material $Al_xGa_{1-x}As$ ($x\simeq0.3$).[15] By applying Löwdin partitioning, the $14\times14$ model can be reduced to models operating in more restricted spaces, e.g., the $8\times8$ $\mathbf{k}\cdot\mathbf{p}$ model (using the basis $\Gamma_{7v}$, $\Gamma_{8v}$, $\Gamma_{6c}$) (Refs. 3 and 16) and a $2\times2$ $\mathbf{k}\cdot\mathbf{p}$ model (for $\Gamma_{6c}$).[3] Löwdin partitioning corresponds to a perturbative treatment of the off-diagonal $\mathbf{k}\cdot\mathbf{p}$ couplings in the $14\times14$ model, which leads to corrections in the reduced models of higher order in $\mathbf{k}$. Consequently, the reduced models are less accurate than the full $14\times14$ model.[3]

In application to quantum well structures, these models are in use with the appropriate modifications (see, e.g., Ref. 13): the material parameters change at the interfaces, in the

 ©1998 The American Physical Society

TABLE I. Material parameters of the 14×14 model for GaAs (Ref. 3) and $Al_xGa_{1-x}As$ (Ref. 15).

| | GaAs | $Al_{0.3}Ga_{0.7}As$ |
|---|---|---|
| $E_0$ (eV) | 1.519 | 1.885 |
| $E_0'$ (eV) | 4.488 | 4504 |
| $\Delta_0$ (eV) | 0.341 | 0.329 |
| $\Delta_0'$ (eV) | 0.171 | 0.165 |
| $\Delta^-$ (eV) | $-0.050i$ | $-0.050i$ |
| $P$ (eV Å) | 10.493 | 10.036 |
| $C_k$ (eV Å) | −0.0034 | −0.0018 |
| $P'$ (eV Å) | $4.780i$ | $4.780i$ |
| $Q$ (eV Å) | 8.165 | 8.165 |
| $m^*$ ($m_0$) | 0.0665 | 0.091 |
| $g^*$ | −0.44 | 0.548 |
| $\gamma_1$ | 6.85 | 5.332 |
| $\gamma_2$ | 2.10 | 1.446 |
| $\gamma_3$ | 2.90 | 2.174 |
| $\kappa$ | 1.20 | 0.582 |
| $q$ | 0.01 | 0.01 |
| $C$ | −1.878 | −1.315 |
| $C'$ | −0.02 | −0.014 |
| $\varepsilon_0$ | 12.40 | 11.698 |
| Conduction band offset (eV) | | 0.240 |

growth direction the wave-vector component $k_z$ is replaced by $(1/i)\partial_z$, and for doped quantum structures the Hartree potential $V_H(z)$ and the exchange-correlation potential $V_{XC}(z)$ (we use the same as in Ref. 7) are added in the diagonal of the $\mathbf{k}\cdot\mathbf{p}$ Hamiltonian. $V_H(z)$ and $V_{XC}(z)$ have to be calculated by self-consistent iteration of the Schrödinger and Poisson equations. An additional parameter in the calculation is the band offset.

It is worth mentioning that the Rashba term in a 2×2 subband Hamiltonian can be obtained in a systematic way by applying Löwdin partitioning to the 14×14 subband Hamiltonian.[13] Similarly, the $k^3$ bulk inversion asymmetry and corresponding interface terms result in the 2×2 subband Hamiltonian as a consequence of higher order perturbation theory applied to the 14×14 model. This concept and its fully self-consistent solution as carried out by Pfeffer and Zawadzki[8] is obviously superior to a merely perturbational treatment of the Rashba and $k^3$ terms with subband states obtained in a parabolic approximation.[7]

The spin-splitting data obtained by inelastic light scattering provide sufficiently accurate and detailed data to test the different models. Here we present self-consistent data from subband calculations based on the 8×8 and 14×14 $\mathbf{k}\cdot\mathbf{p}$ models[13] with material parameters given in Table I. The sample parameters are those given in Table 2 of Ref. 12. In the experiments of Refs. 11 and 12 the spin splitting of the lowest electron subband at the Fermi energy and its dependence on the direction of the in-plane wave vector has been detected for samples with the same nominal width of the quantum well of 180 Å but for different carrier concentrations.

In Fig. 1, we show the conduction-band profile obtained by self-consistent calculation for a 180 Å-wide asymmetrically doped $GaAs/Al_xGa_{1-x}As$ quantum well with a carrier concentration $N_S=8\times10^{11}$ cm$^{-2}$ together with the lowest bound subband levels and the Fermi energy. The self-consistent potential does not depend on whether the 8×8 or 14×14 model is used. With increasing charge carrier densities the potential asymmetry increases. According to our self-consistent calculations, up to $N_S=1.2\times10^{12}$ cm$^{-2}$ all carriers can be accommodated in the lowest subband. These results do not change when we consider a weak unintentional acceptor concentration in the GaAs layer. (In our calculations the depletion charge density $N_d$ was about $10^{10}$ cm$^{-2}$, almost independent of $N_S$.) The spin-degeneracy of all subbands is lifted at finite in-plane wave vector due to BIA and SIA. In Fig. 2, we compare the calculated spin splittings for different in-plane directions from the 8×8 and 14×14 models with the available experimental data. It should be noted, that the experimental data points in our Fig. 2 are those of Fig. 2 in Ref. 12 (converted from cm$^{-1}$ to meV) divided by

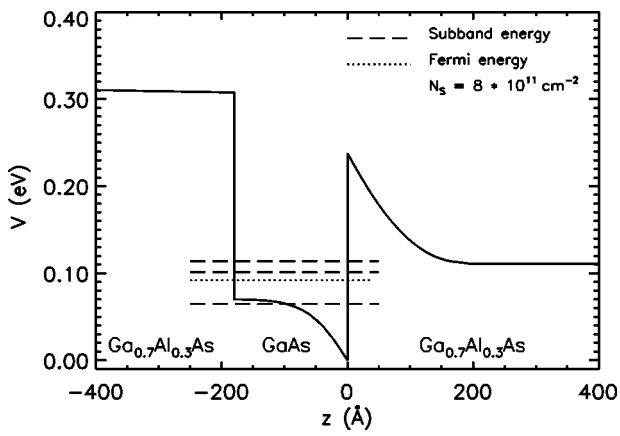


FIG. 1. Conduction-band profile (solid line) of a 180-Å-wide asymmetrically doped $GaAs/Ga_{0.7}Al_{0.3}As$ quantum well with a carrier concentration of $N_S=8\times10^{11}$ cm$^{-2}$. The bottom of the lowest subbands (dashed lines) and the Fermi energy (dotted line) are indicated.

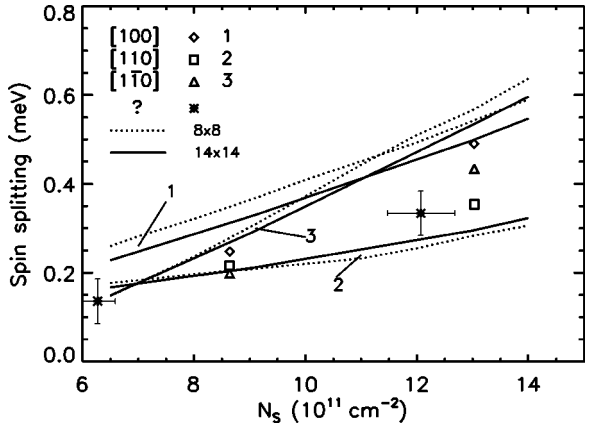


FIG. 2. Calculated spin splittings at the Fermi energy vs carrier concentration for a 180-Å-wide asymmetrically doped $GaAs/Ga_{0.7}Al_{0.3}As$ quantum well for different directions of the in-plane wave vector obtained from the 8×8 (dotted lines) and 14×14 (solid lines) models. Experimental data from Ref. 12 are shown for comparison. For the experimental data points indicated by the asterisks the direction of the in-plane wave vector was not determined.

a factor of 2, because the latter are Raman spin-splittings, which equal twice the subband spin-splitting.

In the experiments of Ref. 12 the electron densities have been determined via the Fermi velocities $v_F$ obtained from the dispersion of the Raman single-particle excitation (SPE) spectrum. The high energy cutoff frequency for SPE of wave vector $\mathbf{q}$ varies as $v_F q$ and was taken as the half maximum point in the high-energy edge of the non-spin-flip SPE line shapes, measured with the polarizations of incident and scattered-light parallel. In Ref. 12 the Fermi velocity has been converted into $k_F$ (and the charge carrier density) using an energy-dependent mass from a $2\times2$ model.[12] The estimated error in the determination of these Fermi velocities of about 2.5% corresponds to an error in the densities of about 5%. The experimental Fermi velocities have been converted into carrier densities by applying a $2\times2$ model.[12] Due to the shortcomings of the $2\times2$ model these densities turn out to be too large if compared with those obtained from the multiband approach. Therefore, the experimental data points in Fig. 2 are shifted to the lower density values, which, according to the present calculation, correspond to the experimentally determined Fermi velocities. The accuracy of the measured Raman spin-splitting ($\pm0.8$ cm$^{-1}$) gives an error of the subband splittings of $\pm0.05$ meV (see Fig. 2).

Considering the fact that the calculations are parameter-free the overall agreement with the measured spin splittings is striking. While for the [110] direction, our results from both models (curves 2) coincide with each other and with the experimental data, there is some model dependence and deviation from the data points for the [100] (curves 1) and $[1\bar{1}0]$ (curves 3) directions with the results from the $14\times14$ model (dash-dotted lines) being closer to the experiment than those from the $8\times8$ model (dotted lines). For the data points denoted by the asterisks the in-plane wave vector was not determined in the experiment. By comparison with our calculation they can be assigned to the [110] direction. The calculated spin splittings turned out to be insensitive to changes in the Al content of the barrier from $x=0.3$ to $x=0.35$, i.e., they would be the same for $x=0.33$, the Al content of the samples in Refs. 11 and 12.

Pfeffer,[8] when applying his $2\times2$ model to the Raman data,[11,12] performs calculations for a single heterojunction. He makes use of the depletion charge density $N_d$ (which usually is not known from experimental data) as a free parameter. With changing $N_d$ from 1.5 to $3.5\times10^{11}$ cm$^{-2}$ he increases the calculated spin splitting, e.g., for the [110] direction, by almost a factor of 2. Pfeffer compares his calculated subband splittings with the experimental data of Fig. 2 in Ref. 12, which are explicitly identified as the measured Raman spin splittings and thus, twice the subband splittings.

In conclusion, we have performed self-consistent subband calculations in the multiband envelope function approach based on $8\times8$ and $14\times14$ $\mathbf{k}\cdot\mathbf{p}$ models for asymmetrically $n$-doped GaAs/Al$_x$Ga$_{1-x}$As quantum wells in order to obtain the spin-splitting at the Fermi energy. Our parameter-free calculations reproduce quantitatively the experimental data obtained from inelastic light scattering both with respect to their dependence on the carrier density and the anisotropy with respect to the direction of the in-plane wave vector. Minor improvements of the results from the $14\times14$ model over those of the $8\times8$ model are found. Given the high accuracy of the bulk band parameters we tend to ascribe the remaining small discrepancies between theory and experiment to uncertainties in the quantum well width and charge carrier concentrations.


[1] C. Kittel, *Quantum Theory of Solids* (Wiley, New York, 1963), p. 184.

[2] E. O. Kane, J. Phys. Chem. Solids **1**, 249 (1957).

[3] U. Rössler, Solid State Commun. **49**, 943 (1984); H. Mayer and U. Rössler, *ibid.* **87**, 81 (1993).

[4] M. Cardona, N. E. Christensen, and G. Fasol, Phys. Rev. B **38**, 1806 (1988).

[5] H. Riechert, S. F. Alvarado, A. N. Titkov, and V. I. Safarov, Phys. Rev. Lett. **52**, 2297 (1984).

[6] Yu. A. Bychkov and E. I. Rashba, J. Phys. C **17**, 6039 (1984).

[7] F. Malcher, G. Lommer, and U. Rössler, Superlattices Microstruct. **2**, 267 (1986); U. Rössler, F. Malcher, and G. Lommer, in *High Magnetic Fields in Semiconductor Physics II*, edited by G. Landwehr (Springer, Berlin, 1989), p. 376.

[8] P. Pfeffer, Phys. Rev. B **55**, R7359 (1997); P. Pfeffer and W. Zawadzki, *ibid.* **52**, R14 332 (1995).

[9] E. A. de Andrada e Silva, G. C. La Rocca, and F. Bassani, Phys. Rev. B **55**, 16 293 (1997).

[10] J. Nitta, T. Akazaki, H. Takayanagi, and T. Enoki, Phys. Rev. Lett. **78**, 1335 (1997); J. P. Heida, B. J. Van Wees, T. M. Klapwijk, and G. Borghs, in *Proceedings of the 23rd International Conference on the Physics of Semiconductors*, edited by M. Scheffler and R. Zimmermann (World Scientific, Singapore, 1996), p. 2467.

[11] B. Jusserand, D. Richards, H. Peric, and B. Etienne, Phys. Rev. Lett. **69**, 848 (1992).

[12] D. Richards, B. Jusserand, G. Allan, C. Priester, and B. Etienne, Solid-State Electron. **40**, 127 (1996); B. Jusserand, D. Richards, G. Allan, C. Priester, and B. Etienne, Phys. Rev. B **51**, 4707 (1995).

[13] R. Winkler and U. Rössler, Phys. Rev. B **48**, 8918 (1993).

[14] P. Pfeffer and W. Zawadzki, Phys. Rev. B **41**, 1561 (1990).

[15] S. Adachi, *GaAs and Related Materials: Bulk Semiconducting and Superlattice Properties* (World Scientific, Singapore, 1994).

[16] H.-R. Trebin, U. Rössler, and R. Ranvaud, Phys. Rev. B **20**, 686 (1979).